



Article

Evaluating the Losses and Recovery of GPP in the Subtropical Mangrove Forest Directly Attacked by Tropical Cyclone: Case Study in Hainan Island

Lan Wu ¹, Enliang Guo ² , Yinghe An ¹, Qian Xiong ¹, Xian Shi ^{1,3}, Xiang Zhang ¹ and Zhongyi Sun ^{1,4,*} ¹ Ecology and Environment College, Hainan University, Haikou 570228, China; wulan@hainanu.edu.cn (L.W.)² College of Geographical Science, Inner Mongolia Normal University, Hohhot 010022, China³ College of Water Conservancy and Electric Power, Heilongjiang University, Harbin 150006, China⁴ Key Laboratory of Agro-Forestry Environmental Processes and Ecological Regulation of Hainan Province, Hainan University, Haikou 570228, China

* Correspondence: gis.rs@hainanu.edu.cn; Tel.: +86-18789989615

Abstract: The gross primary production (GPP) of the mangrove ecosystem determines the upper limit of the scale of its “blue carbon” sink. Tropical cyclones (TCs) are among the most important extreme events that threaten the subtropical mangrove ecosystem and have a serious impact on mangrove ecosystem GPP. However, there are somewhat insufficient scientific findings on regional-scale mangrove ecosystem GPP responding to large-scale weather events such as TCs. Therefore, we selected the subtropical Hainan Island mangrove ecosystem, where more than two TCs pass through per year, as the research area; selected direct-attack TCs as the research object; and took the mangrove vegetation photosynthesis light-use efficiency model established based on the eddy covariance observation data as the tool to evaluate the loss and recovery of mangrove ecosystem GPP after TCs attacked at a regional scale. We found that the TC impacted the mangrove ecosystem GPP through the photosynthetic area and rate, and the recovery of the rate occurred prior to the recovery of the area; the loss of mangrove ecosystem GPP is inversely proportional to the distance to the center of the TC and the distance to the coastline; and the canopy height, diameter at breast height, and aspect where the tree stands significantly influence the response of the mangrove ecosystem GPP to TCs. However, the response varies for different mangrove community compositions, soil conditions, and planting densities as well as different frequencies and intensities of TCs, and they should be analyzed in detail. This study is expected to provide technical and data support for the protection of blue carbon in a subtropical island mangrove ecosystem in response to extreme events and post-disaster recovery.

Keywords: sentinel-2; tropical cyclones; mangrove ecosystem; gross primary production; Hainan Island



Citation: Wu, L.; Guo, E.; An, Y.; Xiong, Q.; Shi, X.; Zhang, X.; Sun, Z. Evaluating the Losses and Recovery of GPP in the Subtropical Mangrove Forest Directly Attacked by Tropical Cyclone: Case Study in Hainan Island. *Remote Sens.* **2023**, *15*, 2094. <https://doi.org/10.3390/rs15082094>

Academic Editors: Tiziana Simoniello and Gabriel Brito Costa

Received: 12 March 2023

Revised: 13 April 2023

Accepted: 13 April 2023

Published: 16 April 2023



Copyright: © 2023 by the authors. Licensee MDPI, Basel, Switzerland. This article is an open access article distributed under the terms and conditions of the Creative Commons Attribution (CC BY) license (<https://creativecommons.org/licenses/by/4.0/>).

1. Introduction

The mangrove ecosystem is a critical component of “blue carbon” due to its high productivity and low rate of decomposition of soil organic carbon, which makes it an effective carbon sink [1,2]. Gross primary production (GPP) is a metric that measures the amount of carbon fixed through photosynthesis in an ecosystem over a specific time period [3]. It provides valuable information on the state of the ecosystem and plays a crucial role in regulating the global carbon cycle, which is the first step in conducting carbon dynamic research [4]. Recent studies have shown that mangrove ecosystems are becoming increasingly vulnerable to climate change [2,5], with more frequent typhoons posing a significant threat [6,7]. Typhoons, or hurricanes depending on where they occur, are collectively referred to as tropical cyclones (TCs). It is essential to improve our understanding of the impact of tropical cyclones on the mangrove ecosystem GPP and evaluate

the recovery capacity. This will improve our comprehension of the interactions between mangrove ecosystems and regional climate change.

Tropical cyclones (TCs), the most reported global disturbance, cause the largest areas of mangrove death [8–12] and directly impact the characteristics of biophysics and biochemistry of mangroves by damaging the mechanical structure [13] and thus reducing mangrove GPP and resilience [14,15]. Research on the impact of TCs on mangroves primarily focuses on several aspects, including biodiversity, community composition, structural and hydrological characteristics, nutrient cycling, vegetation regeneration, and animal community succession [16,17]. The impact of these TCs on mangrove ecosystems has both spatial and temporal dimensions. TCs primarily influence the stand structure and mechanical properties of mangroves through physical damage (e.g., stem breakage, uproot, and trees with internal structural damage or defoliation), then impacting the ecosystem functions [13,18]. Numerous rich scientific findings have found that wind speed is the most significant factor causing damage [19]; the biological characteristics of trees [13,18], such as age, height, crown size and shape, trunk size and shape, wood strength, and root system traits, impact their vulnerability as disaster carriers [18,20]. Meanwhile, factors such as vegetation density, site conditions, and groundwater level influence the exposure of disaster carriers [21], and all three factors jointly determine the form and extent of TC damage to mangroves.

In terms of spatial effects, studies [17,22] mainly concentrate on the damage caused by TCs. The impact of TCs is the most severe near the eye of the storm and generally decreases as the distance from the eye path increases [23,24]. Additionally, areas near open water are more affected than those in the leeward direction [23,24], and the right side tends to be more impacted than the left in the Northern Hemisphere [25], and so on. For the temporal effect, research has mainly focused on the duration and extent of recovery. The recovery of mangrove ecosystems depends on the intensity and frequency of TCs [26,27] and the properties of the ecosystem itself [19]. The recovery of mangroves is mainly the regrowth of surviving trees and the accelerated growth of existing understory species [17,28]. The recovery of severely damaged plant communities, where both aboveground and underground components have been impacted, to their pre-disaster state is difficult [29], while plant communities that experienced only slight disturbance quickly recovered and retained the integrity of the original ecosystem [30]. The resilience of mangrove ecosystems to TCs is substantial, but the ability to recover varies among different tree species [20,31,32]. Moreover, the damage and recovery of mangroves attacked by TCs vary based on factors such as hydrogeomorphology [33], forest type, age structure [34], and the thickness of sediment left by storm surge [35]. The research on the impact of tropical cyclones on mangrove ecosystems and their recovery is abundant, but there are relatively few studies on the carbon dynamics of mangroves before, during, and after tropical cyclones. Especially, there is a lack of quantitative assessments of the impacts of post-disaster mangroves on the carbon cycle at the regional ecosystem scale [36]. The loss of leaves and breakage of trunks lead to the introduction of litter, organic carbon, nitrogen, and other nutrients into the soil, which affects the activity of soil microbes and the supply of nutrients [21]. This impacts the carbon cycle of the mangrove ecosystem [37]. Thus, further research on the impacts of tropical cyclones on subtropical mangrove forest productivity and its post-disturbance is needed to enhance our understanding of the carbon cycle dynamics.

In the view of the assessment process, it is first necessary to know the degree of mangrove damage and the corresponding area. The damaged area can be obtained by remote sensing techniques, but it is difficult to obtain an accurate degree of damage. Field measurements are considered to be a more accurate method, but harsh environmental conditions and high costs often limit their use to providing an estimation of mechanical damage at the quadrat scale [38,39]. Using interpolation methods to upscale this survey to the regional-scale results in significant uncertainties in the estimated loss of GPP [40]. Additionally, using RS-based vegetation indices (VIs), such as the enhanced vegetation index (EVI) and normalized difference vegetation index (NDVI), to estimate the loss of

gross primary production (GPP) may seem like a convenient approach [41], but it also presents the challenge of establishing robust and quantitative relationships between VIs and production [42–44]. Process-based models' simulations can also be utilized to estimate the effect of tropical cyclones on the GPP of the mangrove ecosystem [45]. However, currently, there is significant variability in the results among these models [46]. The functions and parameters of these models are largely based on empirical parameters from terrestrial ecosystems [47], but their applicability to mangrove ecosystems has yet to be validated. Even if using the process-based model specifically for mangroves, the complexity of the data and parameters required would still pose a challenge for the evaluation of the model [45]. The change in GPP of the mangrove ecosystem can be more accurately obtained through the use of the eddy covariance method [39]. However, the effective coverage area of the flux tower is limited to a maximum of a several km radius [48], while the impact of tropical cyclones is much wider, and the damage caused exhibits clear regional differences [23,24]. Combining EC with RS is an effective method for evaluating the GPP of mangrove ecosystems at a regional scale [39,49]. LUE is a more practical approach [50], and among LUEs, the mangrove vegetation photosynthesis light-use efficiency (MVP-LUE), which considers the growth limiting factors of mangrove vegetation, is the model designed to assess the mangrove ecosystem [49]. It has been applied to estimate the GPP of mangrove ecosystems in China across various latitudes and has produced good results.

Climate change is expected to result in an increase in the number of stronger tropical cyclones [51–55]. The changes in tropical cyclone activity are difficult to predict at a regional level [19] and pose a greater threat to the carbon cycle in mangrove ecosystems [56].

Therefore, this study focuses on direct-impact tropical cyclones (excluding tropical depressions and tropical storms with no obvious damage), which have a more significant impact on mangrove ecosystems, and the sub-tropical mangrove distribution area on Hainan Island, which hosts all of China's mangrove species, 20 families and 38 species [57], located on the northern edge of the tropics, as the study area. The objective is to evaluate the impact of tropical cyclones on the GPP of mangrove ecosystems and the subsequent pattern of recovery. The aim is to provide methods to assess the loss of GPP in mangrove ecosystems and the recovery process. This has significant implications for protecting, restoring, and evaluating the role of mangrove ecosystems in the global carbon balance.

2. Materials and Methods

2.1. Study Areas

The study was conducted on Hainan Island, the Northern edge of the tropics ($18^{\circ}10'–20^{\circ}10'N$, $108^{\circ}37'–111^{\circ}03'E$), with a total area of mangrove about 5700 hm^2 (a result of this study) and a coastline of more than 1500 km. The climate in Hainan is a tropical monsoon climate, warm and humid year-round, with an average annual temperature of $22–26^{\circ}C$ and an average rainfall of 1000 to 2600 $mm\ y^{-1}$ [58]. The heaviest rains occur between May and October, always brought by tropical cyclones. Hainan Island is located in the typhoon belt, which is marked by high levels of tropical cyclone activity. On average, Hainan Island is impacted by approximately 7.2 typhoons per year [59].

2.2. Data and Preprocessing

2.2.1. Satellite Data

Sentinel-2 images, including L1C and L2A from both Sentinel-2A and Sentinel-2B, were used in this study [60]. The number of L2A products is very limited; Therefore, if most of the mangroves regions of interest (ROI) can be seen in one scene, we processed L1C to L2A using *sen2cor* in the Sentinel Application Platform (SNAP) [61]. All bands were resampled to 10 m resolution. Sentinel-2 images were adopted for computing the fraction of absorbed photosynthetically active radiation (fAPAR) to estimate the GPP of mangroves, as well as canopy water content (CW), canopy chlorophyll content (CAB), leaf area index (LAI), and a fraction of vegetation cover (fCover) [62] to represent the biochemical and biophysical responses of mangrove ecosystems to tropical cyclones, respectively. From the

performance of results in this study, a total of 68 images from November 2015 to December 2021 were used (for more details, see the Supplementary Material, Table S1). The multi-year monthly fAPAR was derived from the median composition of the corresponding months in non-tropical cyclone years. For any mangrove pixel, if there is no available value for one certain month, then a sliding weighted average of 11-month steps is performed based on the difference between the corresponding month and the multi-year monthly fAPAR.

The Landsat 8 OLI images were obtained from the GEE platform. They were adopted for calculating vegetation indices (VIs) to confirm that the mangroves are in a period of dynamic equilibrium (mature forest). The VIs used in this study include NDVI, EVI, the near-infrared reflectance of vegetation (NIRv) [63], and kernel NDVI (kNDVI) [64]. Each index was calculated for the three years before the selected TC hit (pre-TC) and the three years after the mangrove had completely recovered (post-TC) and compared to determine that the mangroves disturbed by the tropical cyclone are in dynamic balance status, in order to remove the effects of forest growth on GPP. The maximum value composition was utilized by this study to obtain the monthly representation of pre/post-TC. If there were fewer than 3 available images in one ROI of mangrove distribution on a certain month, the calculation was not performed. The available Landsat 8 data used in the present results of this study are Path 27 and Row 07 from 3 May 2013 to 3 December 2021, a total of 60 images; see the Supporting Materials for details (Table S1).

2.2.2. Environmental Data

The environmental data used in this study mainly comprised climatic data and marine hydrographic data, including maximum air temperature (Tmax), mean air temperature (Tem) [65], sea surface temperature (SST) [66], vapor pressure deficit (VPD) [67], sea water salinity (SAL) [68], and photosynthetically active radiation (PAR). Tmax and Tem were sourced from the ERA5 daily air temperature products developed by the European Centre for Medium-Range Weather Forecasts (ECMWF). The daytime air temperature (Tair) was the average of the two. The SST data were also sourced from ECMWF. PAR was obtained from the Global Land Surface Satellite (GLASS). VPD was derived from the TerraClimate dataset, which was created using climatically aided interpolation, combining normal high-spatial-resolution climatological data from historical datasets. We used the Google Earth Engine (GEE) to obtain Hybrid Coordinate Ocean Model (HYCOM) SAL data. HYCOM is a data-assimilative numerical ocean simulation model. This study only utilized the sea surface water salinity data. To match the spatial resolution of the fAPAR from Sentinel-2 images, all the environmental factors were interpolated using the ordinary kriging interpolation. The datasets used in this study are shown in Table 1.

Table 1. Overview of the datasets used in this study.

Data	Period	Resolution		Data Source	Application
		Spatial	Temporal		
Sentinel-2 images	October 2015~December 2020	10 m	5 day	https://scihub.copernicus.eu/dhus/#/home	Estimating GPP Inversing mangrove parameters
landsat 8 OLI images	March 2013~December 2020	30 m	16 day	https://code.earthengine.google.com/	Comparing the status Pre/Post- disturbance
Jilin-1 images	June 2022	0.5 m	-	http://www.jl1.cn/	Mapping mangrove distribution
Inner Mongolia images					
maximum air temperature (Tmax)	2013~2020	0.25°	Daily	https://cds.climate.copernicus.eu/cdsapp#!/search?type=dataset	Estimating GPP
mean air temperature (Tem)					
sea surface temperature (SST)					
sea water salinity (SAL)	2013~2020	0.08°	Daily	https://code.earthengine.google.com/	
vapor pressure deficit (VPD)	2013~2020	~4 km	Monthly	https://code.earthengine.google.com/	
photosynthetically active radiation (PAR)	2013~2020	0.05°	Monthly	http://www.glass.umd.edu/index.html	
Mangroves Map	1996~2022	-	Yearly	https://www.globalmangroveswatch.org	Mapping mangrove distribution
Tropical cyclones data	1949~2021	-	-	https://tcdata.typhoon.org.cn/en/	Screening interfering events

2.2.3. Mangrove Data

Current mangrove distribution: According to the vegetation map of Hainan Island, the distribution range of mangroves was preliminarily determined. Then, we visually interpreted the distribution based on the “Jilin-1” and “Inner Mongolia-1” high-resolution (0.5 m spatial resolution) multi-spectral (RGB and NIR) satellite images purchased from CHANG GUAN Satellite Technology Co. Ltd. (Changchun, China) (<http://www.jl1.cn>, accessed on 15 January 2023), China’s first commercial remote sensing satellite company, which were taken on 22 June 2022. Combining the results of visual interpretation with the field survey of mangrove distribution areas on Hainan Island from June to August 2022 (using drones and manual methods), the distribution of mangroves was finally confirmed.

Historical mangrove distribution: The Global Mangrove Watch (GMW) dataset version 3.0 [69] provides vector data of mangrove distribution in 11 time periods from 1996 to the present and was used to obtain the historical distribution of mangroves in this study (<https://www.globalmangroveswatch.org>, accessed on 15 January 2023). The estimated accuracy of GMW mangrove extent maps was 87.4%. In this study, GMW was utilized to estimate the age range of the directly impacted mangroves and then to ascertain whether they belong to mature forest.

Field data collection: Field surveys were conducted on the mangrove distribution areas impacted by the chosen tropical cyclones, and three sets of 10 × 10 m quadrats were established in the subtidal, intertidal, and supratidal zones. Data collected included diameter at breast height (DBH), canopy height (H), tree density, and so on. The surveys on the distribution of mangrove species and dominant species were manually identified and determined in the entire affected mangrove distribution area. The survey was conducted in August 2022.

2.2.4. Tropical Cyclones Data

Data on tropical cyclones is sourced from the China Meteorological Administration (CMA) Tropical Cyclone Data center (<https://tcdata.typhoon.org.cn/en/>, accessed on 1 June 2022) and the Hainan Province Meteorological Bureau, which provides the “CMA Tropical Cyclone Best Track (TCBT) Dataset” [70] and typhoon disaster data, respectively. TCBT includes 6-hourly track (longitude and latitude of the center) and intensity (minimum air pressure at the center, maximum wind speed near the center, etc.) analyses. The tropical cyclones selected in this study are those whose tracks pass through Hainan Island and its surrounding areas within 5 km from 1949 to 2021. According to the national standard of the “Tropical Cyclone Scale” (GB/T 19201-2006), tropical cyclones are divided into seven categories: 0—weaker than tropical depression, 1—tropical depression (TD, 38.88–61.74 km/h), 2—tropical storm (TS, 61.75–88.02 km/h), 3—strong tropical storm (STS, 88.03–117.54 km/h), 4—typhoon (TY, 117.55–149.22 km/h), 5—strong typhoon (STY, 149.23–183.42 km/h), and 6—super typhoon (SuperTY, ≥ 183.43 km/h).

2.3. Methods

2.3.1. Mangrove Vegetation Photosynthesis Light Use Efficiency Model (MVP-LUE)

The original MVP-LUE (Mangrove vegetation photosynthesis light use efficiency) model was developed by Barr et al. in 2013 and is driven by inputting EVI, PAR, T_{air} , and SAL. However, in this study, we used the improved MVP-LUE model [49] derived by integrating SST on GPP and adding the limit of water condition (VPD) to GPP. Monteith (1972) initially suggested the idea of correlating GPP to PAR via a light use efficiency term (LUE) and multiplicative efficiency factors, which has become the theoretical basis of the LUE model. The theoretical basis of this model is the same as that of the LUE model of typical terrestrial ecosystems; and the method for estimating regional mangrove ecosystem GPP is also the same, scaling up the observations and measurements at EC sites through environmental factors. MVP-LUE not only performed well in the Gulf of Mexico [50], but also estimated the GPP of mangroves in China from 18°N to 28°N and achieved good results [49].

Therefore, MVP-LUE was selected as the tool for GPP estimation in this study, and the parameters were optimized according to the actual field surveys of mangroves on Hainan Island. The model as well as the parameters used to estimate mangrove ecosystem GPP goes as follows:

$$GPP = LUE \times fAPAR \times PAR \quad (1)$$

where GPP is gross primary productivity ($\mu\text{mol C}/\text{m}^2/\text{mon}$); $fAPAR$ is the fraction of PAR absorbed by plant canopy; PAR is the incident photosynthetically active radiation ($\text{mmol}/\text{m}^2/\text{s}$). LUE is the actual light use efficiency ($\text{mol C}/\text{mol PPF}$) which is the maximum LUE (LUE_{\max}) of mangroves regulated by environmental scalars, including T_{air} , SST, SAL, VPD and PAR, as follows:

$$LUE = LUE_{\max} \times T_{air_scalar} \times VPD_{scalar} \times PAR_{scalar} \times SST_{scalar} \times SAL_{scalar} \quad (2)$$

where T_{air_scalar} , SST_{scalar} , VPD_{scalar} , PAR_{scalar} , and SAL_{scalar} are the regulation scalars for the limitation from air and sea water temperature, the water demand, and light and salinity conditions on LUE, respectively. The specific value of LUE_{\max} depends on the range of T_{air} : when T_{air} is within the optimal range for mangrove growth, the LUE_{\max} has the highest value (0.057); conversely, when T_{air} exceeds or falls below the optimal range, the LUE_{\max} is set to 0.047 and 0.055, respectively. The optimal T_{air} varies linearly with latitude, slope = $-0.58^\circ\text{C}/\text{lat}$ ($R^2 = 0.97$, RMSE = 0.39). For the study of mangrove distribution areas in China, it is generally set to 21–25 °C, and in this study, it was set to 22.87–26.05 °C based on the survey data of Hainan Island (see Supporting Materials for details, Figure S1).

The photosynthetic responses of mangroves to SST are similar to T_{air} ; we used the same equation to calculate the scalar. The air temperature dependency factors are defined by Barr et al. [50] as follows:

$$T_{air_scalar} = \frac{(T - T_{min})(T - T_{max})}{(T - T_{min})(T - T_{max}) - (T - T_{opt})^2}, \quad (3)$$

where T_{opt} , T_{max} , and T_{min} are the optimal, maximum and minimum daytime air temperature for the mangrove photosynthetic activities, respectively. Mangroves cannot grow properly when T_{air} is below T_{min} (10 °C), which is the same as the minimum SST of 12 °C, and no photosynthesis occurs below freezing temperature. High temperatures can also reduce the rate of photosynthesis in plants. We set T_{max} and maximum SST to 35 and 32 °C, respectively, according to Zheng and Takeuchi [49]. T_{opt} and optimal SST were set to 28 and 24 °C, respectively.

For VPD_{scalar} ,

$$VPD_{scalar} = \frac{(VPD_{max} - VPD)}{(VPD_{max} - VPD_{min})}, \quad (4)$$

where VPD_{max} (4.0 kPa) and VPD_{min} (0.6 kPa) are the upper and lower limits of VPD for mangroves to adequately develop. If VPD is less than VPD_{min} , there is no restriction of VPD. If VPD is higher than VPD_{max} , the restriction of VPD leads to a photosynthesis rate close to 0.

For PAR and SAL limitation, the equation expressions are same:

$$SAL_{scalar} = 1 - SAL \times m_{sal}, \quad (5)$$

$$PAR_{scalar} = 1 - PAR \times m_{PAR}, \quad (6)$$

where m_{PAR} and m_{sal} (0.0047) present the decreasing rate of scalars to the increasing in response to the increasing PAR and salinity, respectively. The linear function is designed to reflect the PAR constraint on photosynthesis saturation effect by Barr et al. [50]; and the limitations vary depending on the light intensity condition. When PAR is lower than or higher than 1 mmol/m²/s, m_{PAR} is 0.3080 and 0.5171, respectively.

The estimated GPP by MVP-LUE is relatively accurate; comparing the measurements of two EC flux towers in China, the RMSE is 14.25 and 20.40 gC/m²/8 day lower than the MODIS product [49]. MVP-LUE estimates and MODIS GPP products in the study area have also been cross-validated (RMSE = 0.61 and 1.62 gC/m²/day); see Supporting Materials Figure S14 for details.

2.3.2. Tropical Cyclone and Mangroves Screening

First step: This study only focused on directly passing tropical cyclones; those that directly pass-through mangroves will be selected. A 5 km buffer zone is made on both sides of the track of the tropical cyclone. If it intersected with the mangrove distribution area, the tropical cyclone would be selected.

Second step: One of the aims of this study is to propose an effective method for evaluating the GPP loss of mangrove ecosystems caused by typhoons. Typhoons that cause definite damage to mangrove ecosystems are the main research objects in order to achieve better performance. Therefore, if a tropical cyclone passes through the mangrove distribution area and the average wind force near the bottom center reaches level 10 or above (with the condition of trees being uprooted) on the Beaufort wind force scale, the tropical cyclone should be selected.

Third step: The mangrove distribution areas that are directly hit by the selected tropical cyclones were selected.

2.3.3. Quantitative Identification of Influences and Recovery

In the present study, the identification of a year means a cycle year instead of a calendar year. One year is calculated as the twelve months from the month when a TC hits to the previous month of the next year. For example, if a mangrove forest was hit by the typhoon in October 2016, in this situation, the year before typhoon is from October 2015 to September 2016, and the year after the typhoon is from October 2016 to September 2017. The multi-year averaged GPP have been selected as the recovery reference baseline, which is calculated by multi-year averaged monthly environmental condition and the multi-year averaged monthly vegetation state without the TC attack year. In this present study, if the annual GPP exceeded 95% of the baseline value for more than two consecutive years after the TC attacked, then it can be judged that the mangrove ecosystem has recovered. Otherwise, we considered that it is still in the process of recovery. The GPP estimated based on the multi-year average vegetation state and environmental conditions during the recovery period represents the potential GPP during the recovery period. The GPP estimated based on the actual vegetation state and environmental conditions during the same period represents the actual GPP. The estimation of actual, baseline, and potential GPP could be well understood by the flowchart (Figure 1). The difference between these two values indicates the GPP loss caused by TCs.

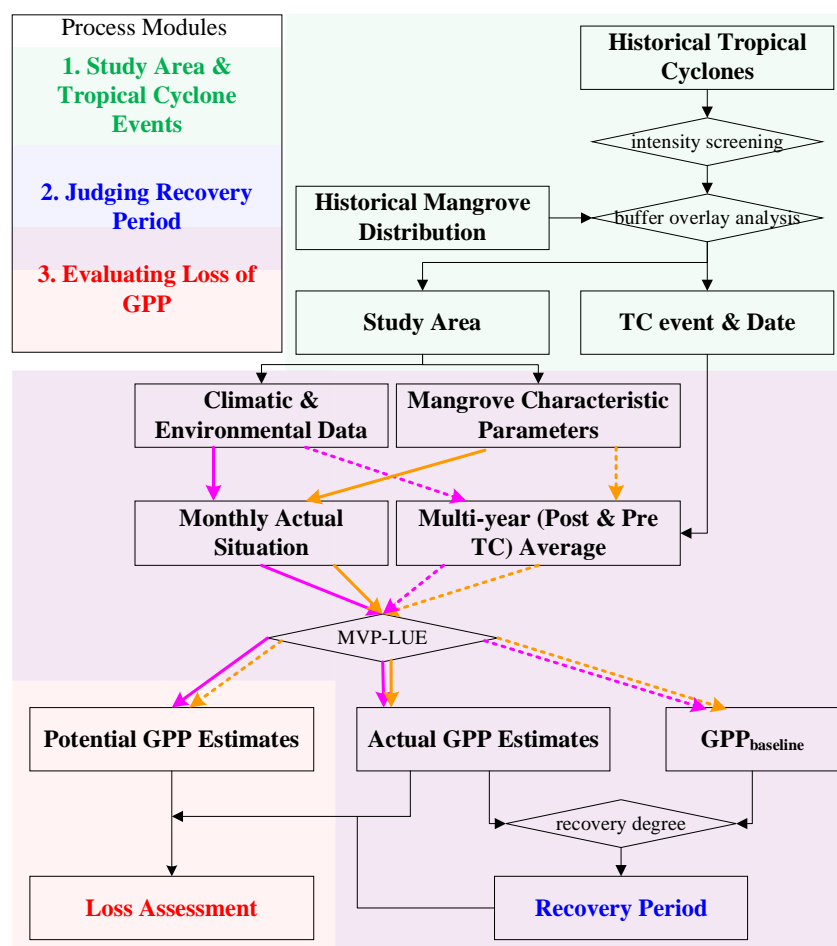


Figure 1. Study flowchart.

3. Results

3.1. The Represent of Tropical Cyclones and Mangroves

From 1949 to 2021, a total of 164 tropical cyclones have hit Hainan Island (see Figures S2 and S3 for detailed paths and years), mainly concentrated in the rainy season of June, July, and August, accounting for 78.17% (Figure S4). From 1949 to 2021, tropical

cyclones have passed through Hainan Island almost every year, with an average of 2.2 times/yr and a maximum of 8 times/yr (1956 and 1971). In terms of levels, there were 12 SuperTY, 14 STY, and 30 TY category typhoons that passed through Hainan Island. The rest of the tropical cyclones did not develop into TY or above. Among them, a total of 26 tropical cyclones hit the mangrove distribution area directly, and there were nine typhoons and above, namely (date): TY: Nona (1 September 1952), Vera (10 July 1983), Willie (16 September 1996); STY: Wanda (25 August 1962), Winnie (24 June 1964), Kelly (27 June 1981); SuperTY: Kate (19 September 1955), Faye (28 August 1963), Sarika (12 October 2016). In order to be representative, according to the screening rule on tropical cyclones and mangroves, “when a tropical cyclone hits a mangrove, the wind speed should be greater than or equal to Beaufort Level 10”. Only SuperTY Sarika finally complied with the standard. Figure 2 shows the force and track of SuperTY Sarika and the mangrove forest it directly hit located across Danzhou Bay, Hainan Island, China. According to the table of “wind speed and force” on the Beaufort scale, when SuperTY Sarika hit the mangrove distribution area in Danzhou Bay, the wind speed reached 110 km/h, belonging to level 11, larger than level 10.

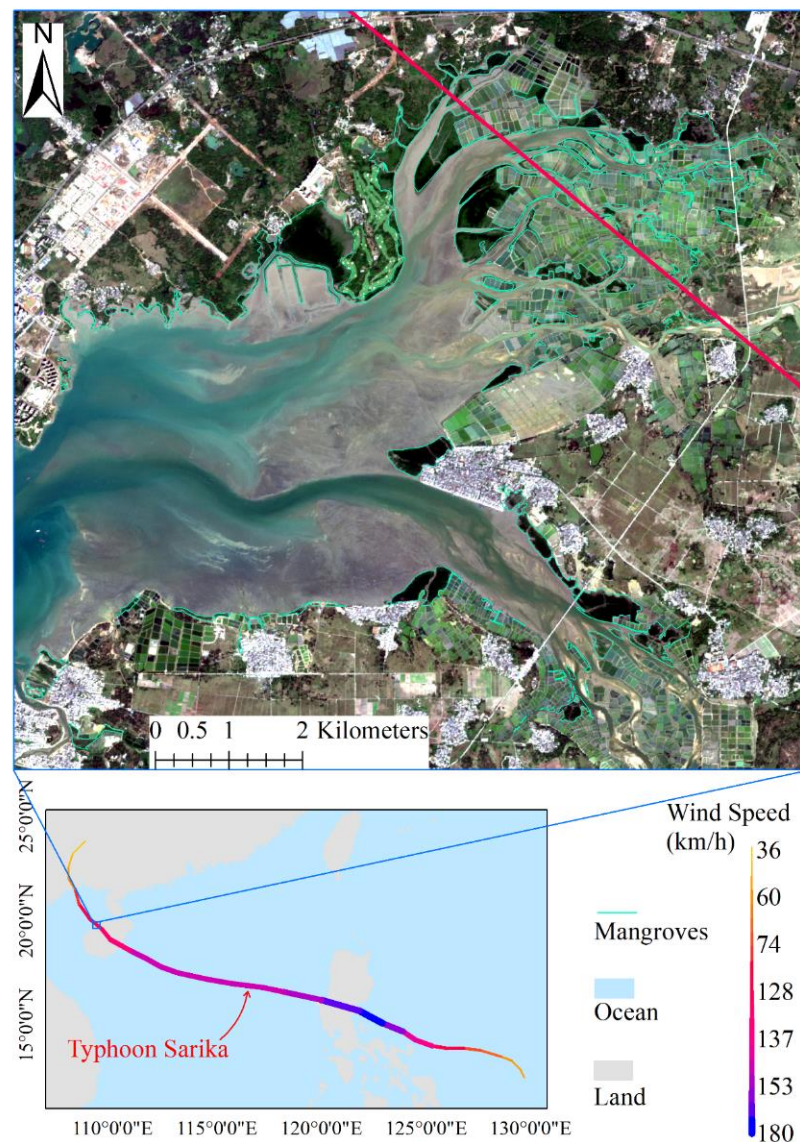


Figure 2. The track of Typhoon Sarika and the mangrove distribution hit by it.

3.2. Recovery of GPP after Tropical Cyclone

The $GPP_{baseline}$, which is the multi-year average annual GPP of mangroves in Danzhou Bay without TC disturbance (SuperTY Sarika in 2016), was $1824.56 \pm 392.72 \text{ gC/m}^2/\text{yr}$ during the study period. Therefore, according to the mangrove recovery rules defined in this study, when the average of GPP of the mangrove ecosystem in Danzhou Bay can reach the standard value of 1732.80 (95% of $GPP_{baseline}$) for two consecutive years, it could then be considered as they have already recovered from disturbance. From 2015 to 2019, the GPP of the mangrove ecosystem in Danzhou Bay were 1848.31 ± 397.22 , 1511.22 ± 371.02 , 1698.01 ± 400.37 , 1844.30 ± 397.40 , and $1808.51 \pm 387.83 \text{ gC/m}^2/\text{yr}$ (spatial distribution can be seen in Figure S5). As shown in Figure 3a, the GPP generated by the mangrove ecosystem in Danzhou Bay in 2016 and 2017 was below the standard value and reached the standard for two consecutive years in 2018 and 2019. Therefore, it is judged that the recovery period was 2 years, and the mangrove ecosystem had recovered in 2018. Among them, from 2016 to 2017, 72.82% of the mangrove ecosystem GPP recovered to 95% of the baseline, and the rest of the mangrove ecosystem is still in the process of recovery; from 2017 to 2018, all mangroves recovered from the SuperTY Sarika impact (Figure 3b). Spatially, combined with Figure 4, the mangroves that recovered relatively quickly are mainly distributed on the inner side of the harbor (the side of the land facing away from the typhoon), while the part exposed to the open water recovered relatively slowly. The GPP of the mangroves farther from the typhoon's track recovered faster than those closer to it. Meanwhile, the mangroves in the same range of distance from the typhoon track, closer to the offshore, recovered faster.

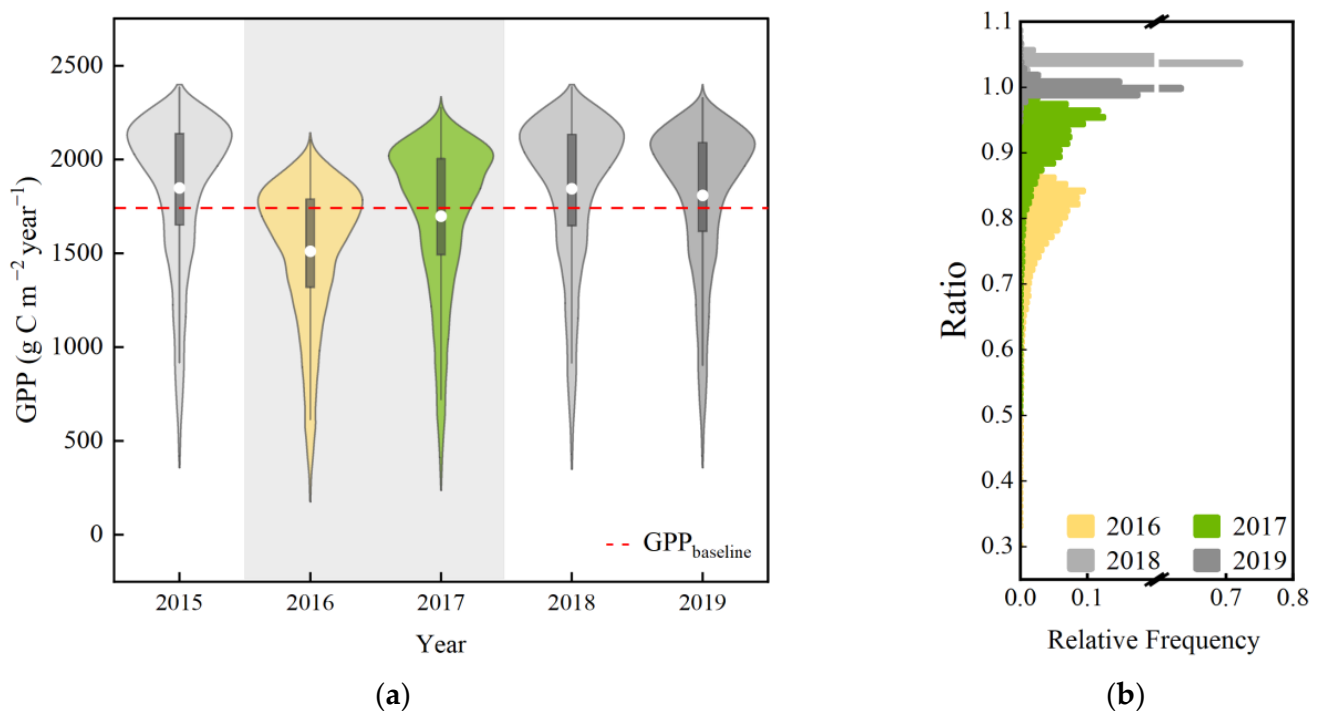


Figure 3. The timeseries of annual GPP of the mangrove ecosystem pre- and post- SuperTY Sarika (a) and the distribution of ratio of each year after the typhoon to the $GPP_{baseline}$ (b).

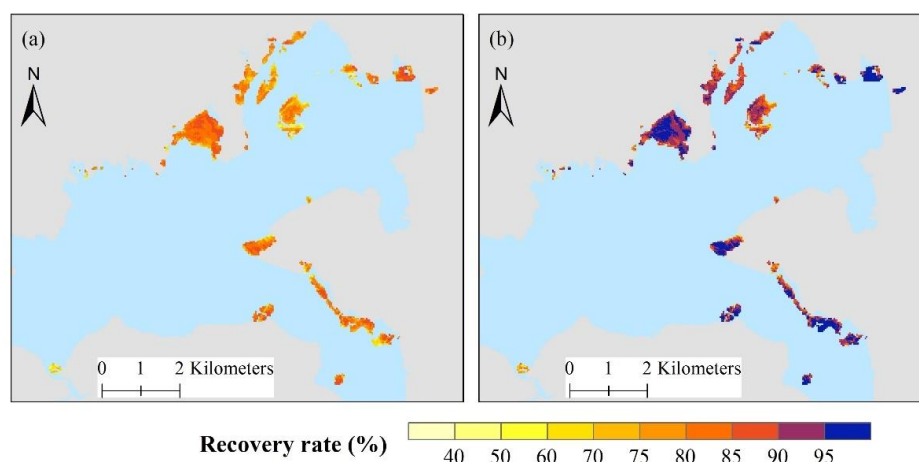


Figure 4. The spatial distribution of GPP recovery rate in the period of two years after Typhoon Sarika hit directly, 2016 (a) and 2017 (b).

3.3. Impact on GPP of Mangrove Forest

The damage brought by SuperTY Sarika to the mangrove GPP in Danzhou Bay lasted for 2 years, and it had recovered to the pre-disturbance state. In the two years, if the mangrove had not been affected by SuperTY Sarika, the GPP of 1683.65 ± 362.85 and 1812.04 ± 387.78 $\text{gC}/\text{m}^2/\text{yr}$ could have been generated. On average, the annual loss of GPP could reach 143.29 ± 84.89 $\text{gC}/\text{m}^2/\text{yr}$, and the most severe area could exceed 600 $\text{gC}/\text{m}^2/\text{yr}$ which was more than half of the multi-year average (loss rate of GPP over 65% and a total of 1294.02 gC/m^2 in two years). Meanwhile, there were also some mangroves not affected by SuperTY Sarika (the average annual loss rate of mangrove forests in 1.92% of the area is less than 1%). The spatial distribution of the annual GPP loss is shown in Figure 3, and the averaged annual loss rate was $8.39 \pm 6.01\%$ /yr. We used the buffer analysis to establish the correlation relationship between the distance to the coastline and the distance to the typhoon eye and GPP loss (Figure 5 subplot). Each point represents the average loss within the 1 km buffer zone, and the five points in the figure are 0~1, 1~2, 2~3, 3~4, and 4~5 km. The loss of mangrove GPP decreased with the increase in the distance to the track of SuperTY Sarika, and the linear average was 21.68 $\text{gC}/\text{m}^2/\text{yr}/\text{km}$ ($R^2 = 0.69$). Simultaneously, the losses increased as the distance to the coastline increased (from land to sea) with the linear average loss rate of 115.42 $\text{gC}/\text{m}^2/\text{yr}/\text{km}$ ($R^2 = 0.78$).

3.4. Dynamic Changes in Mangroves Indices

Blowing down of leaves, breaking of branches, and uprooting are among the several forms of damage to the canopy and community of the mangrove ecosystem caused by the TC, which then affects photosynthesis and ultimately reduces the GPP of the ecosystem. We selected four RS-based parameters, CAB, CW, fCover, and LAI, to represent the damage to the mangrove ecosystem. Figure 6 showed the dynamics of the four indices of the mangroves in Danzhou Bay before and after SuperTY Sarika attacked. The trends of those four parameters are consistent with those in GPP after SuperTY Sarika attacked, with an obvious decline from 2015 to 2016, and an increase in the recovery period from 2016 to 2018. Four parameters became stable after 2018 as well as the spatial distribution (Figure S6). In 2018, the four parameters were all within 95% of the value of pre-TC, and it could be judged that the region basically recovered. The recovery of CW (mean \pm standard deviation from 2015 to 2020: 0.1161 ± 0.1424 , 0.1024 ± 0.1371 , 0.1100 ± 0.1303 , 0.1202 ± 0.1449 , 0.1162 ± 0.1391 , 0.1102 ± 0.1351 g/cm^2) and LAI (2.3884 ± 0.8125 , 1.9282 ± 0.7407 , 2.1174 ± 0.7387 , 2.3358 ± 0.8099 , 2.2788 ± 0.7809 , 2.3163 ± 0.7663 m^2/m^2) were almost linear. CAB (127.5871 ± 59.3427 , 91.3242 ± 46.2653 , 112.4066 ± 54.2731 , 122.7309 ± 57.9359 , 118.8792 ± 53.3375 , 125.3448 ± 55.7427 $\mu\text{g}/\text{cm}^2$) and fCover (0.5890 ± 0.1424 , 0.5231 ± 0.1371 , 0.5252 ± 0.1303 , 0.5774 ± 0.1449 ,

0.5640 ± 0.1391, 0.5679 ± 0.1351) showed the opposite characteristics, where after disturbance CAB recovered quickly in the first year while fCover recovered slowly. fCover could fully recover to the level of pre-TC, while CAB could not. The recovery of fCover is slightly slower than that of CAB in the early stage.

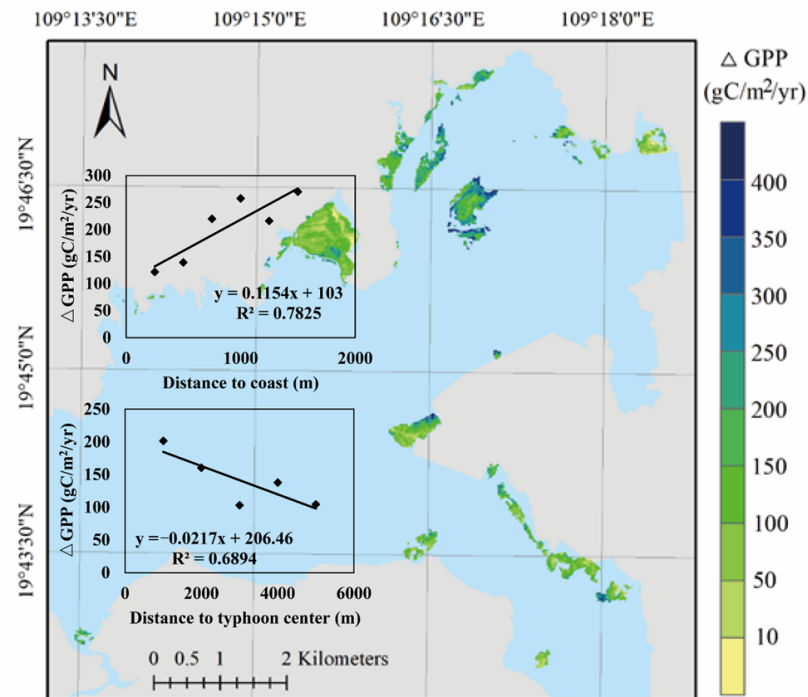


Figure 5. The spatial distribution of GPP annually averaged losses caused by Typhoon Sarika.

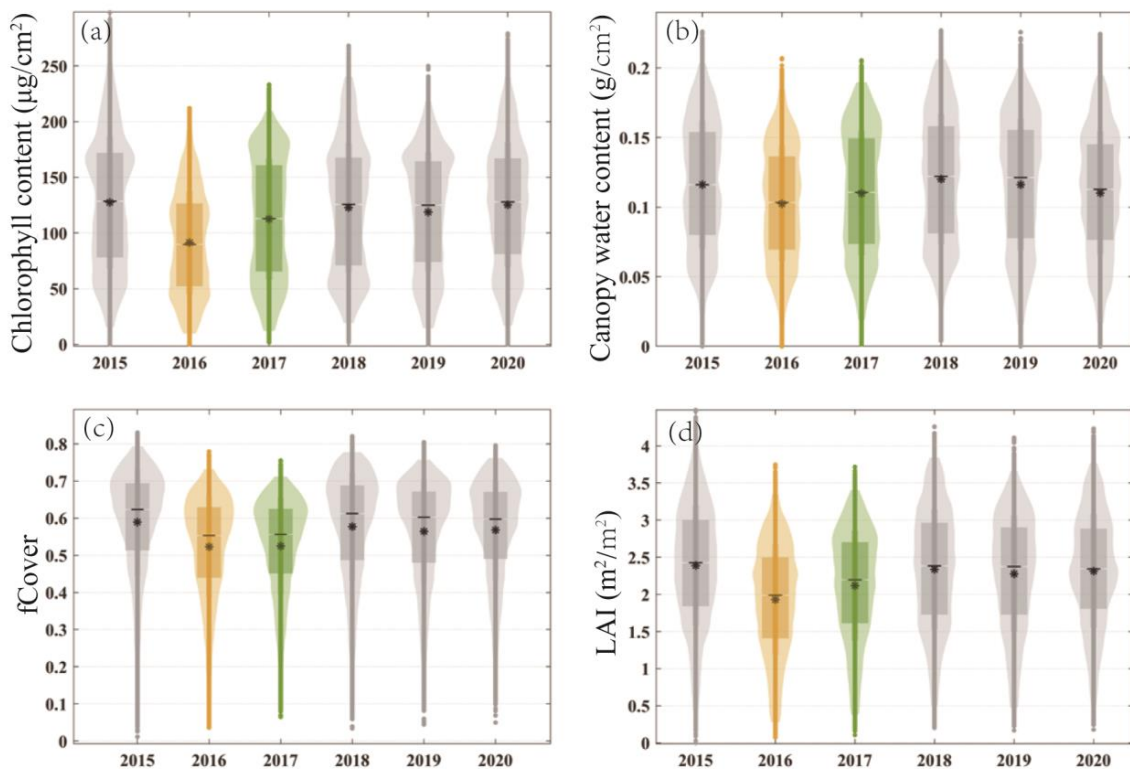


Figure 6. Interannual variations in mangrove canopy parameters (chlorophyll content (a), canopy water content (b), fCover (c) and LAI (d)) from 2015 to 2020.

4. Discussion

4.1. Main Interfering Factors

Eliminating the effects of stand age, phenological rhythm, and meteorological resources: During the process of tree growth, GPP increases with the tree's growth, and this trend will tend toward zero, resulting in a dynamic balance of the whole ecosystem [71]. Additionally, GPP is affected by meteorological conditions and will vary from year to year [4]. Thus, considering the two points mentioned above, it cannot be denied that the high GPP in 2015 was not caused by the advantages of meteorological resources, and the increase in GPP from 2016 to 2018 may also be due to the growth of trees (increases in stand age). To confirm that the reduction from 2015 to 2016 and the uplift from 2016 to 2018 were caused by TC disturbance, we used Global Mangrove Watch to obtain the distribution of mangroves from 1996 to 2020 (Figure S7) and judge the age of the mangroves. We found that the mangroves were mostly older than 20 years. The stand age that GPP reached to the stable period across tree species is different, accounting for 55.56% within 20 years [72]. Temperate tree species generally reach the balance in about 30 years, based on the relationship between the GPP balance period of the boreal and temperate forest [71] and the annual growth period in the tropics leading to faster tree growth; thus, we could deduce that 20-year-old tropical forest could basically reach the GPP equilibrium state. Secondly, we compared the monthly median value composited VIs (including EVI, NDVI, kNDVI, and NIRv) of mangroves before SuperTY Sarika attacked (2013–2015) and after recovery from damage (2018–2020) to eliminate the effect of meteorological factors. In comparing the monthly VIs during the two periods, there was no significant increase or decrease trend (Figures S8–S10).

This study did not compare the images of two scenes before and after SuperTY Sarika attacked to determine the direct damage (e.g., uprooting, broken branches, and scattered leaves), unlike most studies on the vulnerability, loss, and assessment [24,41].

Comparing temporally adjacent images is the common method used in short-term disasters such as fires and typhoons and can complete disaster damage assessment in near real time [41]. Considering that the mangroves were in the growing season when SuperTY Sarika attacked, the inherent phenological rhythm would overestimate the loss; of course, if SuperTY Sarika had occurred in March or April, the inherent phenological rhythm would have underestimated the GPP loss (the monthly loss GPP can be seen in Figures S11 and S12). Therefore, the annual scale GPP was selected as the proxy to determine the legacy effect duration of the TC and quantify the recovery process. It can be judged that the impairment of GPP obtained in this study is mainly caused by the influence of the TC.

4.2. Recovery Period and Legacy Effects

The study estimates that the recovery period is 2 years, but the actual recovery period should be shorter than 2 years (24 months) and longer than 15 months. The recovery period was determined according to the legacy effect duration of the TC on the GPP of mangroves in Danzhou Bay, which was estimated by the values from October to December. What we can definitely infer is that the mangroves had not recovered to pre-disaster state by October–December 2017, but by October–December 2018, the mangroves had recovered to pre-disaster levels. It is undeniable that this study cannot fully determine whether the mangroves have recovered to the pre-disaster level between January 2018 and September 2018. This recovery period is also in line with the recommended survey time of using RS to assess the damage of the typhoon to mangroves within 18 months, the point where fallen leaves and broken branches but also actually surviving trees have basically recovered [73]. However, the recovery of surviving trees does not represent the recovery of ecosystem GPP. Wang et al. [74] and Long et al. [24] investigated the recovery of mangrove forests directly attacked by typhoons in Category 5 on the Saffir–Simpson Scale (significantly stronger than the case in this study); Wang et al. [74] found that, over a period of three years, the mangrove ecosystem could recover fully, and Long et al. [24] used the relationship of

recovery time to estimate that the recovery time of different grades of damage ranged from 24 to 30 months. Small damage and short recovery time are reasonable and can be naturally recovered from in less than five years [75].

We found near linear recovery rates of mangroves for the total damage over time which is consistent with the report of Long et al. [24] that very high R-squared values near 1.0 indicate mangrove damage recovered near linearly for all damage levels but were different from the fast-then-slow pattern of mangrove recovery found in Florida. CW and LAI showed a nearly linear recovery, while CAB showed a trend of a fast-then-slow pattern, which is opposite to fCover change, finally resulting in a nearly linear trend of GPP recovery. Through the recovery patterns of CAB and fCover, it can be inferred that the mangrove ecosystem preferentially obtains a highly efficient unit photosynthesis rate followed by an increase in photosynthetic area.

Due the fact that TCs mainly attack the tropics, the higher cloud cover year-round, and the fewer available images than for the middle and high latitudes [76], the single image taken in one month will have accidental values caused by such factors as the meteorological condition, so in this study, only months with at least three available images were selected in the analysis. Combining satellite imagery, near-Earth UAV aerial photography, and field surveys are recommended to increase the confidence and availability of data. SuperTy Sarika hit Danzhou Bay in October 2016, but due to the limitation that from 2015 to 2020 (the status before and after Sarika hit), not every October had available imagery, we utilized the image composed by the median of all available images from October to December of each year. A t-test was performed on the multi-year monthly images series, and it was possible to determine that there was no significant difference between the three months of October, November, and December. It can be clearly found that both fCover and LAI decreased significantly in 2016, confirming that typhoons can decrease GPP by reducing aboveground biomass, which determine photosynthesis area [77]. The reduction in GPP of the mangrove ecosystem caused by the TC is jointly exerted from the two aspects of ecosystem structure (LAI, fCover) affecting photosynthesis area and material content (CW and CAB) affecting photosynthesis rate. With the gradual recovery of these two aspects during the recovery period, GPP also returned to the pre-disaster state. This is mainly because after the TC, new leaves with stronger photosynthetic rate germinate faster on unbroken branches, while the parts of broken branches and stems (leaf area) recover slowly [78].

4.3. Tree Species and Physical Properties

The physical and chemical properties of mangrove plants are quite different, and the photosynthetic capacity of different mangrove species and the degree of resilience to TCs should differ [19]. It was found that the loss of the *Aegiceras corniculatum* (236.56 ± 126.41) community was higher than that of the *Rhizophora stylosa* + *Aegiceras corniculatum* (173.87 ± 103.10) community, *Rhizophora stylosa* + *Aegiceras corniculatum* + *Avicennia marina* (148.14 ± 93.18) community, *Rhizophora stylosa* (147.48 ± 78.21) community, and *Rhizophora stylosa* + *Avicennia marina* (130.91 ± 69.34) community. Therefore, it can be simply inferred that for typhoon damage, the vulnerability is in the following order: *Aegiceras corniculatum* > *Rhizophora stylosa* > *Avicennia marina*.

There are reports that the degree of forest damage is positively correlated with the height of the stand [18], but the conclusion of this study reveals the opposite (Figure 7a) with a strong correlation ($R = 0.70$), although the finding followed the general results that *Rhizophora* was more severely damaged than *Avicennia* in cases of low-class TCs (*Rhizophora* lower than *Avicennia*) [26,27]. The reasons are that, in terms of wind damage, the studied forest is a dynamic balance forest, the stand heights are relatively consistent, and the probability of wind damage is reduced [79]; Taller mangroves could obtain higher PAR, and their own GPP background value is higher; thus, the loss is greater. Additionally, the surge caused by wind is another major hazard to the mangroves, and the branches and leaves of shorter trees would be directly impacted by the surge, so the damage is greater [23,24]. According to our survey, the GPP loss of the mangrove ecosystem in

Danzhou Bay was also correlated with DBH, and although the quantitative relationship between the DBH and GPP loss was not significant ($p = 0.0659$), the difference in GPP loss of mangroves with different DBH was significant ($p < 0.0001$). On average, the larger the diameter at DBH, the stronger the resistance (Figure 7b). The aspect of mangroves stands is also an important factor; the mangroves growing on the aspect parallel to the direction of typhoon movement are more likely to be damaged by typhoons (SE-NW direction, Figure 7c).

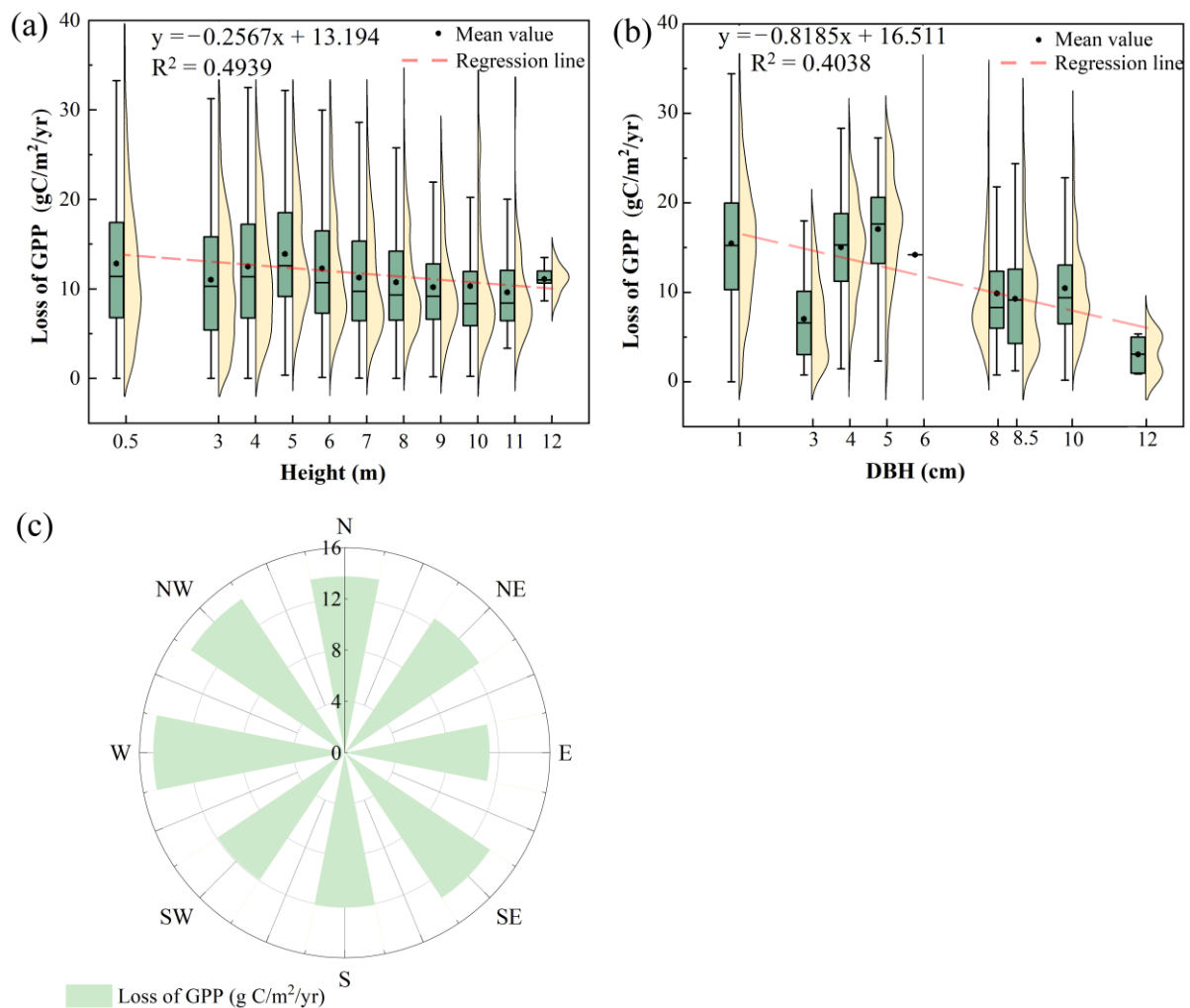


Figure 7. The relationship between loss of GPP and canopy height (a), DBH (b), and aspect (c).

4.4. Uncertainty Analysis

We estimated GPP based on the MVP-LUE model, whose Ta and SST limitations are correlated with each other, which raises the constraints of temperature conditions to a certain extent. This enhanced limit to temperature leads to a lower GPP in 2020 (Figure S5). Secondly, MVP-LUE is an ecosystem-scale model, not a con to several certain mangrove species.

Historical period data are sensitive, so we are unable to obtain the community composition of this area when the typhoon hit in 2016. We only used the results of the field survey in 2022 instead and assumed that the community composition has remained unchanged (with no deeply damaging events such as uprooting that promote regeneration). It is undeniable that our survey is a post-event survey rather than an ex ante one, which also leads to uncertainties. This study did not find the rule of the slope for the mangrove ecosystem GPP in response to the typhoon and did not discuss the environmental condition factors such as soil conditions or the interactive or integrative effects. It is noteworthy that even for the

same tree species, the different stand ages and densities lead to different responses to the TC of the same level [19]; at the same time, the environmental conditions of mangrove growth are the key factors that cause different losses of mangroves [80]. The influences should be interactive. This study did not deeply and quantitatively assess the hazards of causing factors since only one case of a direct typhoon was obtained according to the screening rules, such as the typhoon intensity and other factors that have not been considered.

5. Conclusions

This study collected all tropical cyclones (TCs) that attacked Hainan Island from 1949 to 2021, combined with the historical distribution of mangrove forests, to complete the screening of the study area and the attacking TCs. Using Sentinel imagery and the MVP-LUE model, the gross primary production (GPP) loss and recovery of object mangrove ecosystems directly attacked by TCs were estimated, and the following main conclusions were obtained: The RS-based MVP-LUE process proposed in this study is an efficient and effective way to assess the GPP damage and post-disaster recovery at the regional or ecosystem scale. TCs affect the GPP of the mangrove ecosystem via both the reduction in photosynthesis rate and area, and the recovery of the photosynthesis rate per unit area was faster than that of the photosynthesis area. The farther the distance to the coastline and to the center of TCs, the lower the GPP loss, showing an almost linear weakening trend. The canopy height, the DBH, the standing aspect, and their integrative effects are closely related to the loss of GPP. In this case, this study focused on Danzhou Bay, attacked by SuperTY Sarika in 2016, and the GPP of the mangroves ecosystem can recover to the state pre-TC within two years.

However, the process of the loss and recovery of GPP in mangrove ecosystems with different stand ages, community compositions, etc., under the effects of typhoons with different intensities and directions should not be the same and should be analyzed specifically for each case.

Supplementary Materials: The following supporting information can be downloaded at: <https://www.mdpi.com/article/10.3390/rs15082094/s1>, Figure S1: The relationship between the optimal photosynthesis temperature and latitudes of mangrove ecosystem [81–85]; Table S1: valid satellite images in this study; Figure S2: The historical trajectories of each category of tropical cyclones hit Hainan Island from 1949 to 2021; Figure S3: Historical records of tropical cyclones that hit Hainan Island; Figure S4: Intra-annual distribution of various tropical cyclones; Figure S5: The annual GPP in Danzhou Bay from 2013 to 2020 (using the multi-year average vegetation parameters to estimate GPP in 2013 and 2014); Figure S6: The yearly changes of canopy parameters of mangrove forest from 2015 to 2020; Figure S7: The historical spatial distribution of mangrove in Danzhou Bay; Figure S8: The differences of RS-based VIs between the three years pre-SuperTY Sarika and that in the three years post-SuperTY Sarika, in Area 1; Figure S9: The differences of RS-based VIs between the three years pre-SuperTY Sarika and that in the three years post-SuperTY Sarika, in Area 2; Figure S10: The differences of RS-based VIs between the three years pre-SuperTY Sarika and that in the three years post-SuperTY Sarika, in Area 3; Figure S11: The spatial distribution of monthly GPP in the first year after SuperTY Sarika hit; Figure S12: The spatial distribution of monthly GPP in the second year after SuperTY Sarika hit; Figure S13: Interannual variations in mangrove fAPAR from 2015 to 2020; Figure S14: Cross-validation with MODIS products.

Author Contributions: Conceptualization, Z.S. and Y.A.; data curation, analysis and methodology, Z.S., E.G. and Q.X.; visualization, X.S. and Y.A.; writing—original draft preparation, L.W. and X.Z.; project administration, L.W.; funding acquisition, Z.S. and L.W. All authors have read and agreed to the published version of the manuscript.

Funding: This research was supported by Hainan Provincial Natural Science Foundation, High-level talent project (322RC580) and Hainan Province's key development plan project (ZDYF2022SHFZ111).

Data Availability Statement: The data from this study could be provided to readers interested in the relevant research period. Please contact the corresponding author Z.S. with a reasonable request.

Acknowledgments: The authors would like to thank the editors and the anonymous reviewers for their crucial comments, which improved the quality of this paper. We are also very grateful to Wei Cui from National Forestry and Grassland Administration of China, Peng Wang and Quan Chen from Hainan University and Junfu Zhao from Hainan Provincial Ecological Environment Monitoring Center for their help during the field survey.

Conflicts of Interest: The authors declare no conflict of interest.

References

- Danielsen, F.; Sørensen, M.K.; Olwig, M.F.; Selvam, V.; Parish, F.; Burgess, N.D.; Hiraishi, T.; Karunakaran, V.M.; Rasmussen, M.S.; Hansen, L.B.; et al. The Asian tsunami: A protective role for coastal vegetation. *Science* **2005**, *310*, 643. [CrossRef] [PubMed]
- Alongi, D.M. The impact of climate change on mangrove forests. *Curr. Clim. Chang. Rep.* **2015**, *1*, 30–39. [CrossRef]
- Beer, C.; Reichstein, M.; Tomelleri, E.; Ciais, P.; Jung, M.; Carvalhais, N.; Rödenbeck, C.; Arain, M.A.; Baldocchi, D.; Bonan, G.B.; et al. Terrestrial gross carbon dioxide uptake: Global distribution and covariation with climate. *Science* **2010**, *329*, 834–838. [CrossRef] [PubMed]
- Sun, Z.; Wang, X.; Zhang, X.; Tani, H.; Guo, E.; Yin, S.; Zhang, T. Evaluating and comparing remote sensing terrestrial GPP models for their response to climate variability and CO₂ trends. *Sci. Total Environ.* **2019**, *668*, 696–713. [CrossRef]
- Ward, R.D.; Friess, D.A.; Day, R.H.; MacKenzie, R.A. Impacts of climate change on mangrove ecosystems: A region by region overview. *Ecosyst. Health Sustain.* **2016**, *2*, e01211. [CrossRef]
- Kathiresan, K.; Rajendran, N. Coastal mangrove forests mitigated tsunami. *Estuar. Coast. Shelf Sci.* **2005**, *65*, 601–606. [CrossRef]
- Dahdouh-Guebas, F.; Jayatissa, L.; Di Nitto, D.; Bosire, J.; Seen, D.L.; Koedam, N. How effective were mangroves as a defence against the recent tsunami? *Curr. Biol.* **2005**, *15*, R443–R447. [CrossRef]
- Lindroth, A.; Lagergren, F.; Grelle, A.; Klemetsson, L.; Langvall, O.; Weslien, P.; Tuulik, J. Storms can cause Europe-wide reduction in forest carbon sink. *Glob. Chang. Biol.* **2009**, *15*, 346–355. [CrossRef]
- Adame, M.F.; Kauffman, J.B.; Medina, I.; Gamboa, J.N.; Torres, O.; Caamal, J.P.; Reza, M.; Herrera-Silveira, J.A. Carbon stocks of tropical coastal wetlands within the karstic landscape of the Mexican Caribbean. *PLoS ONE* **2013**, *8*, e56569. [CrossRef]
- Reichstein, M.; Bahn, M.; Mahecha, D.M.; Kattge, J.; Baldocchi, D.D. Linking plant and ecosystem functional biogeography. *Proc. Natl. Acad. Sci. USA* **2014**, *111*, 13697–13702. [CrossRef]
- Pilli, R.; Grassi, G.; Kurz, W.A.; Moris, J.V.; Viñas, R.A. Modelling forest carbon stock changes as affected by harvest and natural disturbances. II. EU-level analysis. *Carbon Balance Manag.* **2016**, *11*, 20. [CrossRef] [PubMed]
- Uriarte, M.; Thompson, J.; Zimmerman, J.K. Hurricane María tripled stem breaks and doubled tree mortality relative to other major storms. *Nat. Commun.* **2019**, *10*, 1362. [CrossRef]
- Herrera-Silveira, J.A.; Teutli-Hernandez, C.; Secaira-Fajardo, F.; Braun, R.; Bowman, J.; Geselbracht, L.; Guerra Cano, L. *Hurricane Damages to Mangrove Forests and Post-Storm Restoration Techniques and Costs*; The Nature Conservancy: Arlington, TX, USA, 2022. [CrossRef]
- Zhang, K.; Thapa, B.; Ross, M.; Gann, D. Remote sensing of seasonal changes and disturbances in mangrove forest: A case study from South Florida. *Ecosphere* **2016**, *7*, e01366. [CrossRef]
- Murdiyarto, D.; Purbopuspito, J.; Kauffman, J.B.; Warren, M.W.; Sasmito, S.D.; Donato, D.C.; Manuri, S.; Krisnawati, H.; Taberima, S.; Kurnianto, S. The potential of Indonesian mangrove forests for global climate change mitigation. *Nat. Clim. Chang.* **2015**, *5*, 1089–1092. [CrossRef]
- Herbert, D.A.; Fownes, J.H.; Vitousek, P.M. Vitousek. Hurricane damage to a Hawaiian forest: Nutrient supply rate affects resistance and resilience. *Ecology* **1999**, *80*, 908–920. [CrossRef]
- Baldwin, A.; Egnatovich, M.; Ford, M.; Platt, W. Regeneration in fringe mangrove forests damaged by Hurricane Andrew. *Plant Ecol.* **2001**, *157*, 151–164. [CrossRef]
- Islebe, G.A.; Torrescano-Valle, N.; Valdez-Hernández, M.; Tuz-Novelo, M.; Weissenberger, H. Efectos del Impacto del Huracán Dean en la Vegetación del Sureste de Quintana Roo, México. *For. Veracruzana* **2009**, *11*, 1–6. Available online: <https://www.redalyc.org/articulo.oa?id=49711999001> (accessed on 1 June 2022).
- Krauss, K.W.; Osland, M.J. Tropical cyclones and the organization of mangrove forests: A review. *Ann. Bot.* **2020**, *125*, 213–234. [CrossRef]
- Imbert, D. Hurricane disturbance and forest dynamics in east Caribbean mangroves. *Ecosphere* **2018**, *9*, e02231. [CrossRef]
- Taillie, P.J.; Roman-Cuesta, R.; Lagomasino, D.; Cifuentes-Jara, M.; Fatoyinbo, T.L.; Ott, E.L.; Poulter, B. Widespread mangrove damage resulting from the 2017 Atlantic mega hurricane season. *Environ. Res. Lett.* **2020**, *15*, 064010. [CrossRef]
- Platt, W.J.; Doren, R.F.; Armentano, T.V. Effects of Hurricane Andrew on stands of slash pine (*Pinus elliottii* var. *densa*) in the everglades region of south Florida (USA). *Plant Ecol.* **2000**, *146*, 43–60. [CrossRef]
- Carrillo-Bastos, A.; Elizalde-Rendón, E.M.; Valle, N.T.; Ortiz, G.F. Adaptación ante disturbios naturales, manglar de Puerto Morelos, Quintana Roo, México. *For. Veracruzana* **2008**, *10*, 31–38. Available online: <http://www.redalyc.org/articulo.oa?id=49711434004> (accessed on 1 June 2022).
- Long, J.; Giri, C.; Primavera, J.; Trivedi, M. Damage and recovery assessment of the Philippines' mangroves following Super Typhoon Haiyan. *Mar. Pollut. Bull.* **2016**, *109*, 734–743. [CrossRef]

25. Stanturf, J.A.; Goodrick, S.L.; Outcalt, K.W. Disturbance and coastal forests: A strategic approach to forest management in hurricane impact zones. *For. Ecol. Manag.* **2007**, *250*, 119–135. [[CrossRef](#)]
26. Imbert, D.; Labbé, P.; Rousteau, A. Hurricane damage and forest structure in Guadeloupe, French West Indies. *J. Trop. Ecol.* **1996**, *12*, 663–680. [[CrossRef](#)]
27. Galeano, A.; Urrego, L.E.; Botero, V.; Bernal, G. Mangrove resilience to climate extreme events in a Colombian Caribbean Island. *Wetl. Ecol. Manag.* **2017**, *25*, 743–760. [[CrossRef](#)]
28. Smith, T.J.; Robblee, M.B.; Wanless, H.R.; Doyle, T.W. Mangroves, hurricanes, and lightning strikes. *BioScience* **1994**, *44*, 256–262. [[CrossRef](#)]
29. Baldwin, A.H.; Mendelsohn, I.A. Mendelsohn. Response of two oligohaline marsh communities to lethal and nonlethal disturbance. *Oecologia* **1998**, *116*, 543–555. [[CrossRef](#)]
30. Kauffman, J.B.; Cole, T.G. Micronesian mangrove forest structure and tree responses to a severe typhoon. *Wetlands* **2010**, *30*, 1077–1084. [[CrossRef](#)]
31. Feller, I.C.; Dangremond, E.M.; Devlin, D.J.; Lovelock, C.E.; Proffitt, C.E.; Rodriguez, W. Nutrient enrichment intensifies hurricane impact in scrub mangrove ecosystems in the Indian River Lagoon, Florida, USA. *Ecology* **2015**, *96*, 2960–2972. [[CrossRef](#)]
32. Villamayor, B.M.R.; Rollon, R.N.; Samson, M.S.; Albano, G.M.G.; Primavera, J.H. Impact of Haiyan on Philippine mangroves: Implications to the fate of the widespread monospecific *Rhizophora* plantations against strong typhoons. *Ocean Coast. Manag.* **2016**, *132*, 1–14. [[CrossRef](#)]
33. Han, X.; Feng, L.; Hu, C.; Kramer, P. Hurricane-induced changes in the Everglades National Park mangrove forest: Landsat observations between 1985 and 2017. *J. Geophys. Res. Biogeosci.* **2018**, *123*, 3470–3488. [[CrossRef](#)]
34. Sherman, R.E.; Martinez, P.; Fahey, T.J. Hurricane impacts on a mangrove forest in the Dominican Republic: Damage patterns and early recovery 1. *Biotropica* **2001**, *33*, 393–408. [[CrossRef](#)]
35. Ellison, J. Impacts of sediment burial on mangroves. *Mar. Pollut. Bull.* **1999**, *37*, 420–426. [[CrossRef](#)]
36. Hernandez, J.O.; Maldia, L.S.; Park, B.B. Research trends and methodological approaches of the impacts of windstorms on forests in tropical, subtropical, and temperate zones: Where are we now and how should research move forward? *Plants* **2020**, *9*, 1709. [[CrossRef](#)] [[PubMed](#)]
37. Liechty, H.O.; Jurgensen, M.F.; Mroz, G.D.; Gale, M.R. Pit and mound topography and its influence on storage of carbon, nitrogen, and organic matter within an old-growth forest. *Can. J. For. Res.* **1997**, *27*, 1992–1997. [[CrossRef](#)]
38. Giri, C.; Ochieng, E.; Tieszen, L.L.; Zhu, Z.; Singh, A.; Loveland, T.; Masek, J.; Duke, N. Biogeography. Status and distribution of mangrove forests of the world using earth observation satellite data. *Glob. Ecol. Biogeogr.* **2011**, *20*, 154–159. [[CrossRef](#)]
39. Wang, L.; Jia, M.; Yin, D.; Tian, J. A review of remote sensing for mangrove forests: 1956–2018. *Remote Sens. Environ.* **2019**, *231*, 111223. [[CrossRef](#)]
40. Virkkala, A.-M.; Aalto, J.; Rogers, B.M.; Tagesson, T.; Treat, C.C.; Natali, S.M.; Watts, J.D.; Potter, S.; Lehtonen, A.; Mauritz, M.; et al. Statistical upscaling of ecosystem CO₂ fluxes across the terrestrial tundra and boreal domain: Regional patterns and uncertainties. *Glob. Chang. Biol.* **2021**, *27*, 4040–4059. [[CrossRef](#)]
41. Tran, T.V.; Reef, R.; Zhu, X. A Review of Spectral Indices for Mangrove Remote Sensing. *Remote Sens.* **2022**, *14*, 4868. [[CrossRef](#)]
42. Pham, T.D.; Yokoya, N.; Bui, D.T.; Yoshino, K.; Friess, D.A. Remote sensing approaches for monitoring mangrove species, structure, and biomass: Opportunities and challenges. *Remote Sens.* **2019**, *11*, 230. [[CrossRef](#)]
43. Nguyen, H.-H.; Nguyen, T.T.H. Above-ground biomass estimation models of mangrove forests based on remote sensing and field-surveyed data: Implications for C-PFES implementation in Quang Ninh Province, Vietnam. *Reg. Stud. Mar. Sci.* **2021**, *48*, 101985. [[CrossRef](#)]
44. Guo, X.; Wang, M.; Jia, M.; Wang, W. Estimating mangrove leaf area index based on red-edge vegetation indices: A comparison among UAV, WorldView-2 and Sentinel-2 imagery. *Int. J. Appl. Earth Obs. Geoinf.* **2021**, *103*, 102493. [[CrossRef](#)]
45. Yoshikai, M.; Nakamura, T.; Suwa, R.; Sharma, S.; Rollon, R.; Yasuoka, J.; Egawa, R.; Nadaoka, K. Predicting mangrove forest dynamics across a soil salinity gradient using an individual-based vegetation model linked with plant hydraulics. *Biogeosciences* **2022**, *19*, 1813–1832. [[CrossRef](#)]
46. Friedlingstein, P.; Jones, M.W.; O’Sullivan, M.; Andrew, R.M.; Bakker, D.C.; Hauck, J.; Le Quéré, C.; Peters, G.P.; Peters, W.; Pongratz, J.; et al. Global carbon budget 2021. *Earth Syst. Sci. Data* **2022**, *14*, 1917–2005. [[CrossRef](#)]
47. Rivera-Monroy, V.H.; Zhao, X.; Wang, H.; Xue, Z.G. Are Existing Modeling Tools Useful to Evaluate Outcomes in Mangrove Restoration and Rehabilitation Projects? A Minireview. *Forests* **2022**, *13*, 1638. [[CrossRef](#)]
48. Sun, Z.; Wang, X.; Yamamoto, H.; Tani, H.; Zhong, G.; Yin, S. An attempt to introduce atmospheric CO₂ concentration data to estimate the gross primary production by the terrestrial biosphere and analyze its effects. *Ecol. Indic.* **2018**, *84*, 218–234. [[CrossRef](#)]
49. Zheng, Y.; Takeuchi, W. Estimating mangrove forest gross primary production by quantifying environmental stressors in the coastal area. *Sci. Rep.* **2022**, *12*, 2238. [[CrossRef](#)]
50. Barr, J.G.; Engel, V.; Fuentes, J.D.; Fuller, D.O.; Kwon, H. Modeling light use efficiency in a subtropical mangrove forest equipped with CO₂ eddy covariance. *Biogeosciences* **2013**, *10*, 2145–2158. [[CrossRef](#)]
51. Knutson, T.R.; McBride, J.L.; Chan, J.; Emanuel, K.; Holland, G.; Landsea, C.; Held, I.; Kossin, J.P.; Srivastava, A.K.; Sugi, M. Tropical cyclones and climate change. *Nat. Geosci.* **2010**, *3*, 157–163. [[CrossRef](#)]

52. Knutson, T.R.; Sirutis, J.J.; Zhao, M.; Tuleya, R.E.; Bender, M.; Vecchi, G.A.; Villarini, G.; Chavas, D. Global projections of intense tropical cyclone activity for the late twenty-first century from dynamical downscaling of CMIP5/RCP4. 5 scenarios. *J. Clim.* **2015**, *28*, 7203–7224. [CrossRef]
53. Christensen, J.H.; Kanikicharla, K.K.; Aldrian, E.; An, S.I.; Cavalcanti, I.F.A.; de Castro, M.; Dong, W.; Goswami, P.; Hall, A.; Kanyanga, J.K. *Climate Phenomena and Their Relevance for Future Regional Climate Change: In Climate Change 2013 the Physical Science Basis: Working Group I Contribution to the fifth Assessment Report of the Intergovernmental Panel on Climate Change*; Cambridge University Press: Cambridge, UK, 2014; pp. 1217–1308. [CrossRef]
54. Sobel, A.H.; Camargo, S.J.; Hall, T.M.; Lee, C.-Y.; Tippett, M.K.; Wing, A.A. Human influence on tropical cyclone intensity. *Science* **2016**, *353*, 242–246. [CrossRef] [PubMed]
55. Patricola, C.M.; Wehner, M.F. Anthropogenic influences on major tropical cyclone events. *Nature* **2018**, *563*, 339–346. [CrossRef]
56. Kossin, J.P.; Knapp, K.R.; Olander, T.L.; Velden, C.S. Global increase in major tropical cyclone exceedance probability over the past four decades. *Proc. Natl. Acad. Sci. USA* **2020**, *117*, 11975–11980. [CrossRef] [PubMed]
57. Fang, F.; Li, Z.; Gui, H. Investigation and Research on Current Situation of Mangrove in Hainan. *Trop. For.* **2022**, *50*, 42–49. [CrossRef]
58. Cui, W.; Xiong, Q.; Zheng, Y.; Zhao, J.; Nie, T.; Wu, L.; Sun, Z. A Study on the Vulnerability of the Gross Primary Production of Rubber Plantations to Regional Short-Term Flash Drought over Hainan Island. *Forests* **2022**, *13*, 893. [CrossRef]
59. Xiao, F.; Liu, Q. An evaluation of vegetation loss due to the super typhoon Sarika in Hainan Island of China. *Nat. Hazards* **2022**, *115*, 1677–1695. [CrossRef]
60. Drusch, M.; Del Bello, U.; Carlier, S.; Colin, O.; Fernandez, V.; Gascon, F.; Hoersch, B.; Isola, C.; Laberinti, P.; Martimort, P.; et al. Sentinel-2: ESA's optical high-resolution mission for GMES operational services. *Remote Sens. Environ.* **2012**, *120*, 25–36. [CrossRef]
61. Main-Knorn, M.; Pflug, B.; Louis, J.; Debaecker, V.; Müller-Wilm, U.; Gascon, F. Sen2Cor for sentinel-2. In Proceedings of the SPIE Remote Sensing, Warsaw, Poland, 4 October 2017. [CrossRef]
62. Weiss, M.; Baret, F. S2ToolBox Level 2 Products: LAI, FAPAR, FCOVER, Version 1.1. 2016. Available online: http://step.esa.int/docs/extra/ATBD_S2ToolBox_L2B_V1.1.pdf (accessed on 1 June 2022).
63. Badgley, G.; Field, C.B.; Berry, J.A. Canopy near-infrared reflectance and terrestrial photosynthesis. *Sci. Adv.* **2017**, *3*, e1602244. [CrossRef]
64. Camps-Valls, G.; Campos-Taberner, M.; Moreno-Martínez, A.; Walther, S.; Duveiller, G.; Cescatti, A.; Mahecha, M.D.; Muñoz-Marí, J.; García-Haro, F.J.; Guanter, L.; et al. A unified vegetation index for quantifying the terrestrial biosphere. *Sci. Adv.* **2021**, *7*, eabc7447. [CrossRef]
65. ERA5: Fifth Generation of ECMWF Atmospheric Reanalyses of the Global Climate. Available online: <https://cds.climate.copernicus.eu/cdsapp#!/home> (accessed on 8 March 2023).
66. Hirahara, S.; Alonso-Balmaseda, M.; de Boissesson, E.; Hersbach, H. *26 Sea Surface Temperature and Sea Ice Concentration for ERA5*; European Centre for Medium Range Weather Forecasts: Reading, UK, 2016.
67. Abatzoglou, J.T.; Dobrowski, S.; Parks, S.A.; Hegewisch, K.C. TerraClimate, a high-resolution global dataset of monthly climate and climatic water balance from 1958–2015. *Sci. Data* **2018**, *5*, 170191. [CrossRef]
68. Chassignet, E.P.; Hurlburt, H.E.; Smedstad, O.M.; Halliwell, G.R.; Hogan, P.J.; Wallcraft, A.J.; Baraille, R.; Bleck, R. The HYCOM (hybrid coordinate ocean model) data assimilative system. *J. Mar. Syst.* **2007**, *65*, 60–83. [CrossRef]
69. Bunting, P.; Rosenqvist, A.; Hilarides, L.; Lucas, R.M.; Thomas, N.; Tadono, T.; Worthington, T.A.; Spalding, M.; Murray, N.J.; Rebelo, L.-M. Global mangrove extent change 1996–2020: Global Mangrove Watch version 3.0. *Remote Sens.* **2022**, *14*, 3657. [CrossRef]
70. Lu, X.; Yu, H.; Ying, M.; Zhao, B.; Zhang, S.; Lin, L.; Bai, L.; Wan, R. Western North Pacific tropical cyclone database created by the China Meteorological Administration. *Adv. Atmos. Sci.* **2021**, *38*, 690–699. [CrossRef]
71. Tang, J.; Luysaert, S.; Richardson, A.D.; Kutsch, W.; Janssens, I.A. Steeper declines in forest photosynthesis than respiration explain age-driven decreases in forest growth. *Proc. Natl. Acad. Sci. USA* **2014**, *111*, 8856–8860. [CrossRef]
72. He, L.; Chen, J.M.; Pan, Y.; Birdsey, R.; Kattge, J. Relationships between net primary productivity and forest stand age in US forests. *Glob. Biogeochem. Cycles* **2012**, *26*, GB3009. [CrossRef]
73. Primavera, J.; Cruz, M.D.; Montilijao, C.; Consunji, H.; Paz, M.D.; Rollon, R.; Maranan, K.; Samson, M.; Blanco, A. Preliminary assessment of post-Haiyan mangrove damage and short-term recovery in Eastern Samar, central Philippines. *Mar. Pollut. Bull.* **2016**, *109*, 744–750. [CrossRef]
74. Wang, Y. Detecting Vegetation Recovery Patterns after Hurricanes in South Florida Using NDVI Time Series. Master's Thesis, University of Miami, Coral Gables, FL, USA, 2012.
75. Danielson, T.M.; Rivera-Monroy, V.H.; Castañeda-Moya, E.; Briceño, H.; Travieso, R.; Marx, B.D.; Gaiser, E.; Farfán, L.M. Assessment of Everglades mangrove forest resilience: Implications for above-ground net primary productivity and carbon dynamics. *For. Ecol. Manag.* **2017**, *404*, 115–125. [CrossRef]
76. Shrestha, D.P.; Saepuloh, A.; van der Meer, F. Land cover classification in the tropics, solving the problem of cloud covered areas using topographic parameters. *Int. J. Appl. Earth Obs. Geoinf.* **2019**, *77*, 84–93. [CrossRef]
77. Wu, L.; Kato, T.; Sato, H.; Hirano, T.; Yazaki, T. Sensitivity analysis of the typhoon disturbance effect on forest dynamics and carbon balance in the future in a cool-temperate forest in northern Japan by using SEIB-DGVM. *For. Ecol. Manag.* **2019**, *451*, 117529. [CrossRef]

78. Walker, L.R. Tree damage and recovery from Hurricane Hugo in Luquillo experimental forest, Puerto Rico. *Biotropica* **1991**, *23*, 379–385. [[CrossRef](#)]
79. Mitchell, S.J.; Hailemariam, T.; Kulis, Y. Empirical modeling of cutblock edge windthrow risk on Vancouver Island, Canada, using stand level information. *For. Ecol. Manag.* **2001**, *154*, 117–130. [[CrossRef](#)]
80. Smith, T.J.; Anderson, G.H.; Balentine, K.; Tiling, G.; Ward, G.A.; Whelan, K.R.T. Cumulative impacts of hurricanes on Florida mangrove ecosystems: Sediment deposition, storm surges and vegetation. *Wetlands* **2009**, *29*, 24–34. [[CrossRef](#)]
81. Leopold, A.; Marchand, C.; Renchon, A.; Deborde, J.; Quiniou, T.; Allenbach, M.J.A.; Meteorology, F. Net ecosystem CO₂ exchange in the “Coeur de Voh” mangrove, New Caledonia: Effects of water stress on mangrove productivity in a semi-arid climate. *Agric. For. Meteorol.* **2016**, *223*, 217–232. [[CrossRef](#)]
82. Pongparn, S.; Komiyama, A.; Umnouysin, S.; Rodtassana, C.; Sangtiewan, T.; Maknual, C.; Pravinvongvuthi, T.; Suchewaboripont, V.; Kato, S.J.F. Ten-year estimation of net primary productivity in a mangrove forest under a tropical monsoon climate in eastern Thailand: Significance of the temperature environment in the dry season. *Forests* **2020**, *11*, 987. [[CrossRef](#)]
83. Chen, L.; Wang, W.; Li, Q.Q.; Zhang, Y.; Yang, S.; Osland, M.J.; Huang, J.; Peng, C.J.E. Mangrove species’ responses to winter air temperature extremes in China. *Ecosphere* **2017**, *8*, e01865. [[CrossRef](#)]
84. Qiaomin, Z.; Shuzhen, S.; Yechun, Z.; Hongbing, Y.U.; Zongxun, S.; Xiaosheng, W. Marine environmental indexes related to mangrove growth. *Acta Ecol. Sin.* **2001**, *21*, 1427–1437. [[CrossRef](#)]
85. Huang, X.-L.; Pend, X.; Qiu, J.B.; Chen, S.B. Mangrove status and development prospects in southern Zhejiang Province. *J. Zhejiang For. Coll.* **2009**, *26*, 7. [[CrossRef](#)]

Disclaimer/Publisher’s Note: The statements, opinions and data contained in all publications are solely those of the individual author(s) and contributor(s) and not of MDPI and/or the editor(s). MDPI and/or the editor(s) disclaim responsibility for any injury to people or property resulting from any ideas, methods, instructions or products referred to in the content.